Reference to published article:
Vessey, C.J., Schmidt, M. P., Abdolahnezhad, M., Peak, D. & Lindsay, M. B. J. (2020). Adsorption of (Poly)vanadate onto Ferrihydrite and Hematite: An In Situ ATR–FTIR Study. *ACS Earth and Space Chemistry*, 4(4): 641–649. https://doi.org/10.1021/acsearthspacechem.0c00027

Adsorption of (poly)vanadate onto ferrihydrite and hematite: An *in-situ* ATR-FTIR study

Colton J. Vessey,[a†] Michael P. Schmidt,[b] Mojtaba Abdolahnezhad,[a] Derek Peak,[b] Matthew B. J. Lindsay[a,*]

[a] *Department of Geological Sciences, University of Saskatchewan, Saskatoon, Saskatchewan, S7N 5E2, Canada*

[b] *Department of Soil Sciences, University of Saskatchewan, Saskatoon, Saskatchewan, S7N 2V3, Canada*

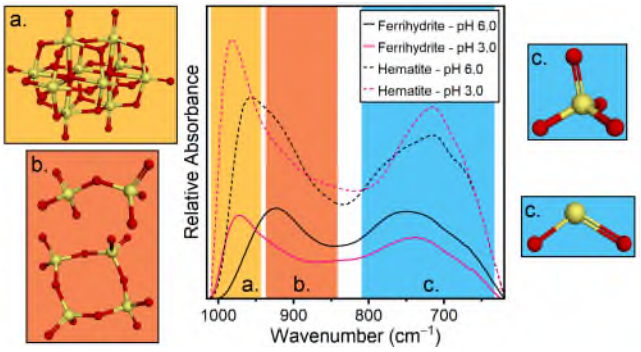

TOC/Abstract Art.

* Corresponding author: Tel: +1 306 966 5693; Fax: +1 306 966 8593

E-mail address: matt.lindsay@usask.ca (M.B.J. Lindsay)

Keywords: vanadium; polymerization; ferrihydrite; hematite; adsorption; ATR-FTIR; surface complexation

ABSTRACT

Vanadium (V) has been a useful trace metal in describing Earth's biogeochemical cycling and development of industrial processes; however, V has recently been recognized as a potential contaminant of concern. Although Fe (oxyhydr)oxides are important sinks for aqueous V in soils and sediments, our understanding of adsorption mechanisms is currently limited to mononuclear species (i.e., $H_xVO_4^{(3-x)-}$). Here we use *in situ* attenuated total reflectance – Fourier transform infrared spectroscopy to examine sorption mechanisms and capacity for (poly)vanadate attenuation by ferrihydrite and hematite from pH 3 to 6. Adsorption isotherms illustrate the low affinity of polyvanadate species for ferrihydrite surfaces compared to hematite. Mononuclear V species (i.e., $[H_xVO_4]^{(3-x)-}$ and VO_2^+) were present at all experimental conditions. At low surface loadings and pH 5 and 6, $H_2VO_4^-$ adsorption onto ferrihydrite and hematite surfaces results from formation of inner-sphere complexes. At $[V]_T$ above 250 μM, adsorbed polynuclear V species in this study include $H_2V_2O_7^{2-}$ and $V_4O_{12}^{4-}$. Whereas, $HV_{10}O_{28}^{6-}$, $H_3V_{10}O_{28}^{5-}$, and $NaHV_{10}O_{28}^{4-}$ are the predominant adsorbed species at pH 3 and 4 and elevated $[V]_T$. Surface polymers were identified on hematite at all experimental pH values, whereas polymeric adsorption onto ferrihydrite was limited to pH 3 and 4. These results suggest that hematite offers a more suitable substrate for polymer complexation compared to ferrihydrite. Our results demonstrate the pH- and concentration-dependant removal of (poly)vanadate species by Fe(III) (oxyhydr)oxides, which has implications for understanding V mobility, behaviour, and fate in the environment.

INTRODUCTION

Vanadium (V) is a redox sensitive trace metal that has a wide range of applications from industrial processes (e.g., catalysis), manufacturing (e.g., steel works), and as a paleo-indicator for studying Earth's biogeochemical cycles.[1–4] Background crustal concentrations generally range from 95 to 300 mg kg^{-1}, however, concentrations exceeding 1000 mg kg^{-1} are commonly associated with primary ore minerals and secondary phases in bauxite, phosphate, coal, black shales, and crude oil deposits at elevated concentrations.[4–6] Vanadium can be acutely toxic to organisms and has recently been listed as a contaminant of concern due to increased anthropogenic release from industrial (i.e., steel byproducts or catalytic chemistry), mining activities, and fossil fuel combustion.[7–11] Vanadium is listed in USEPA Contaminant Candidate List 4,[12] yet few jurisdictions have established water quality guidelines (e.g., Canada and the Netherlands).[13,14] While background aqueous V concentrations range from 0.0005 to 180 μg L^{-1}, depending on the weathering rates and source material, concentrations have been shown to exceed 1 mg L^{-1} in mining environments.[15–17]

Aqueous V speciation is highly dependant on redox conditions, pH, total vanadium concentration ($[V]_T$) and ionic strength (I), with a variety of monomeric and polymeric species possible under different conditions.[5,18,19] Under oxic conditions, V(V) dominates and forms monomeric ($[H_xVO_4]^{(3-x)-}$) and polymeric (e.g., $[H_xV_{10}O_{28}]^{(6-x)-}$) aqueous species. With increasing $[V]_T$, oligomerization and condensation reactions produce dimers ($[H_xV_2O_7]^{(4-x)-}$), trimers ($V_3O_{10}^{5-}$), tetramers ($V_4O_{12}^{4-}$), pentamers ($V_5O_{15}^{5-}$), hexamers ($V_6O_{18}^{6-}$), and decamers ($[H_xV_{10}O_{28}]^{(6-x)-}$) between pH 2 and 9. At low (< 2) and high (> 9) pH, polynuclear species decompose to form VO_2^+ and HVO_4^{2-}, respectively. Unlike octahedrally coordinated molybdenum (Mo) and tungsten (W) polynuclear species, polyvanadate species have a tetrahedral coordination, with the

exception of octahedral decavanadate. Aqueous polyvanadate species form corner-sharing VO_4 tetrahedra connected by bridging O atoms to form $[H_xV_2O_7]^{(4-x)-}$, or cyclical $V_4O_{12}^{4-}$, $V_5O_{15}^{5-}$, and $V_6O_{18}^{6-}$ structures.[10,20] In comparison, the decavanadate structure includes three distinct octahedral sites.[10,18,20] This structure includes six V atoms in the middle, two of which are in the center (site a) and differ from the other four surrounding V atoms (site b), these six atoms are then capped by two atoms at the top and bottom (site c).

Iron (Fe) (oxyhydr)oxides are a key control on element mobility and bioavailability in soils and sediments.[21] These phases exhibit a high affinity for uptake of oxyanion-forming elements, including V, by sorption or incorporation reactions.[22–29] Sorption of mononuclear vanadate species onto Fe(III) (oxyhydr)oxides results from formation of inner-sphere bidentate corner- and edge-sharing surface complexes.[22,25,26,29] While aqueous vanadate sorption by Fe(III) (oxyhydr)oxides has been described previously in field and laboratory settings,[16,22,23,25,26,29–32] the interaction of aqueous polynuclear V species with these phases has not been examined. Nevertheless, these reactions likely impact V mobility in terrestrial waters characterized by elevated $[V]_T$ or low pH conditions. Previous studies have utilized *in situ* attenuated total reflectance-Fourier transform infrared (ATR-FTIR) spectroscopy to examine adsorption of polynuclear Mo(VI), W(VI), and U(VI) onto Fe(III) (oxyhydr)oxides and layered double hydroxides.[33–37] For example, attenuation of mono and polynuclear Mo(VI) species by hematite occurred through monodentate, bidentate, and tridentate sorption complexes, and additionally formed surface polymers by epitaxial growth on crystalline (0001) hematite surfaces.[38] Formation of surface polymers at Fe(III) (oxyhydr)oxide surfaces can inhibit the adsorption of inorganic contaminants and, therefore, decrease the reactivity of natural iron phases.[39–41]

Several studies have used X-ray absorption spectroscopy to probe mechanisms of vanadate ($H_2VO_4^{2-}$) uptake 2-line ferrihydrite and hematite,[23,25,29] yet polyvanadate species have not previously been considered. Here we use *in situ* ATR FTIR spectroscopy examine adsorption of aqueous (poly)vanadate species by 2-line ferrihydrite [$5Fe_2O_3 \cdot 9H_2O$] (ferrihydrite) and nano-hematite [α-Fe_2O_3] (hematite) over a range of pH (3 to 6) and $[V]_T$ (50 to 5000 μM) conditions. We perform thermodynamic modelling to predict relative proportions of (poly)vanadate species and, therefore, to inform interpretation of ATR-FTIR results. Analysis of molecular-level reactions between aqueous monomeric, oligomeric, and polymeric species and mineral surfaces by ATR-FTIR is a well-established technique.[35,41–45] Our results contribute new information on aqueous (poly)vanadate attenuation by Fe(III) (oxyhydr)oxides and improve understanding of processes controlling V abundance and distribution in soils and sediments.

MATERIALS AND METHODS

Materials and Synthesis. Solutions were prepared using ultra-pure water (18.2 MΩ cm^{-1} resistivity) that was boiled for 15 min, cooled, and purged with $N_{2(g)}$ for 24 h in an anoxic chamber (Coy Laboratories, 5% H_2 balanced with N_2) to limit dissolved CO_2 and dissolved carbonate species during ATR-FTIR experiments. A stock solution containing 5000 μM V was prepared by dissolving high purity (>99.0%) sodium orthovanadate (Na_3VO_4) in a 0.05 M NaCl background electrolyte. This stock solution was then diluted to produce a range of $[V]_T$: 50, 100, 250, 500, 750, 1000, 3000, and 5000 μM. The pH of these solutions was then adjusted with 0.1 or 1.0 M trace-metal grade HCl to pH (± 0.1) 3, 4, 5, or 6.

Ferrihydrite and hematite synthesis followed methods described by Cornell and Schwertmann (2003) and Al-Kady et al. (2011) with slight modifications. Briefly, ferrihydrite was synthesized by dissolving 40 g of $FeCl_3$ in 500 mL of deionized (DI) water and titrated with 1.0 M NaOH to

pH 7.5 and stirred vigorously for 1 h. Hematite was prepared by dissolving $FeCl_3$ in boiling deionized water, which was allowed to react for 30 min, at which time concentrated NaOH was added until pH stabilized at pH 7 and allowed to cool at room temperature. Resulting ferrihydrite and hematite suspensions were centrifuged and rinsed at least 3 times with DI water to remove residual ions. Synthesized ferrihydrite and hematite phases were confirmed by XRD and prior to *in situ* flow experiments by collecting baseline ATR-FTIR spectra of deposited ferrihydrite or hematite films. The solids were then resuspended in 0.05 M NaCl electrolyte to achieve a 10 g L^{-1} mineral slurry.

***In situ* ATR-FTIR Isotherm Experiments.** ATR-FTIR spectra were collected on an Invenio-R FTIR spectrometer (Bruker Corp., USA) equipped with an N_2-cooled HgCdTe (MCT) detector. Measurements were collected with a Bruker Platinum ATR with a single-bounce ZnSe/diamond internal reflective element (IRE) with a 45° incidence angle. The instrument and sample compartments were continuously purged with dry air. Spectra represent an average of 512 scans collected at 4 cm^{-1} resolution. Collected FTIR spectra were truncated between 620 to 1010 cm^{-1}, baseline corrected, and integrated using OPUS v.8.1 software. The truncation limits selected to minimize distortion from baseline correction and to avoid interference of unavoidable bands from H_2O and Fe (oxyhydr)oxide present below ~600 cm^{-1}. At ~667 cm^{-1} a small negative band relating to CO_2 is present, but overall does not affect the interpretation or deconvolution fits for adsorbed spectra.

Initial spectra were collected for aqueous V samples at 5000 μM for pH 1, 4, 7, and 11. The selected pH values were selected to observe aqueous VO_2^+, $H_xV^VO_4^{(3-x)-}$, and polynuclear species, which correspond to distinct IR bands. A background scan was obtained for the 0.05 M NaCl background electrolyte and sample spectra were then collected by dropping aqueous V

samples onto the IRE. Adsorption isotherm experiments were performed by equilibrating V(V) solutions (50 to 5000 μM) with ferrihydrite and hematite films under constant flow. Films deposited on the ATR crystal were done by drop casting 10 μL of prepared mineral suspensions (10 g L^{-1}) and dried under continuous flow of $N_{2(g)}$ until no residual water was apparent. The drop casting procedure was repeated until complete coverage of the IRE was achieved. Following deposition of ferrihydrite or hematite, the 0.05 M NaCl background solution was passed over the film at a constant rate of 1.3 mL min^{-1} using a peristaltic pump (FH100 Peristaltic Pump, Thermo Scientific); this process was repeated for each pH. An initial background spectrum was collected, and spectra were then recorded every 2 min until the film reached equilibration with the electrolyte, noticed by lack of changes in the spectra. Following equilibration, a background spectrum was collected and vanadate solutions were systematically introduced from low (50 μM) to high (5000 μM) $[V]_T$. Spectra were collected every 60 s to monitor adsorption of (poly)vanadate species onto ferrihydrite and hematite at each $[V]_T$ until steady state was achieved (20 to 30 min). Once a steady state was reached the next highest V solution was passed through the setup. Band positions were identified by 2nd derivative analysis of each spectra at the given pH conditions. Processed spectra were then integrated to produce adsorption isotherms for each given pH condition following reaction with ferrihydrite and hematite films. Integrated isotherm areas for each system were fit using the Langmuir isotherm equation by inverse modeling to minimize the root-mean-square error (RMSE). Deconvolution of spectra was achieved by fitting the minimum number of Gaussian peaks using the Origin software package (Origin V.2016).

Aqueous Speciation Modeling. Thermodynamic equilibrium modeling of aqueous V species was performed using the PHREEQCi (Version 3.1.5) code with a modified Minteq version 3.1

database.[47,48] Vanadium speciation was modeled using the Davies activity model in a 0.05 M NaCl background electrolyte. Mononuclear and polynuclear V protonation reactions and equilibrium constants were also considered from Baes and Mesmer[18], Cruywagen et al.[20,49], Elvingson et al.[50], Larson[51], McCann et al.[52,53], Smith et al.[54] and compared to the Minteq database (Table S1).[47] Aqueous Na-decavanadate ($NaH_xV_{10}O_{28}^{(5-x)-}$) complexes can represent up to ~40 % of the total V species at 5000 μM and low ionic strength (I = 0.05 M), and were therefore considered in thermodynamic modeling (Table S1).[19,47,54]

RESULTS

ATR-FTIR Spectra. Initial aqueous V spectra collected at pH 1, 4, 7, and 11 displayed distinct features associated with the VO_2^+, $H_xV^VO_4^{(3-x)-}$, and polynuclear species (Figure 1 and S1) and were consistent with literature values summarized in Table 1. A broad band at 1187 cm^{-1} with weak shoulders at 938 and 1015 cm^{-1} is apparent in spectra for the pH 1 solution. Spectra collected for the pH 4 solution exhibit weak bands at 842, 965, and 1016 cm^{-1}, whereas at pH 7 bands were present at 834, 952, and 1066 cm^{-1}. A single band is present at 861 cm^{-1} in spectra obtained for the pH 11 solution.

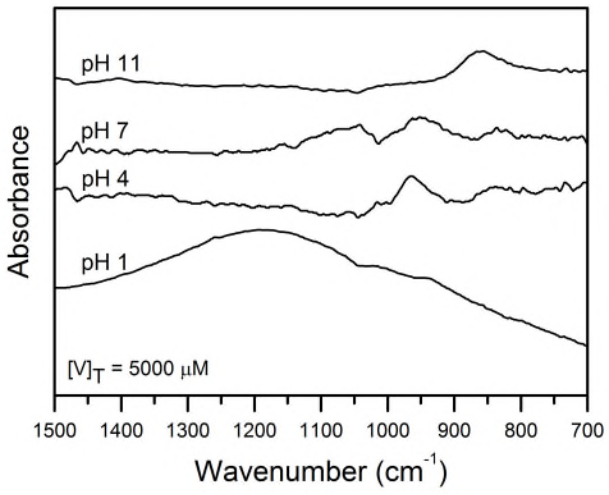

Figure 1. ATR-FTIR spectra for solutions containing 5000 μM V(V) adjusted to pH 11, 7, 4, and 1. Spectra collected at pH 7 and 4 were expanded by 3x.

Multiple bands are apparent in spectra obtained during vanadate sorption onto ferrihydrite and hematite from pH 3 to 6 (Figure 2). Band positions were determined from minima in the 2nd derivative of adsorbed spectra and optimized by deconvolution fits (Figure 3; Table S2). Vanadium adsorption onto ferrihydrite produced broader spectral features and fewer bands regardless of concentration (Figure 2). Bands are apparent at 660, 711, 764, 815, 885, and 935 cm^{-1} at pH 6 following reaction with ferrihydrite. The bands at 660, 711, and 764 cm^{-1} exhibit relatively consistent position and intensity across all pH values, whereas bands positioned between 800 and 1000 cm^{-1} shift to higher frequencies with decreasing pH. This trend also applies to new bands at 977 cm^{-1} (pH 3) and 970 cm^{-1} (pH 4), which increase in intensity as pH decreases and $[V]_T$ increases (Figure 3).

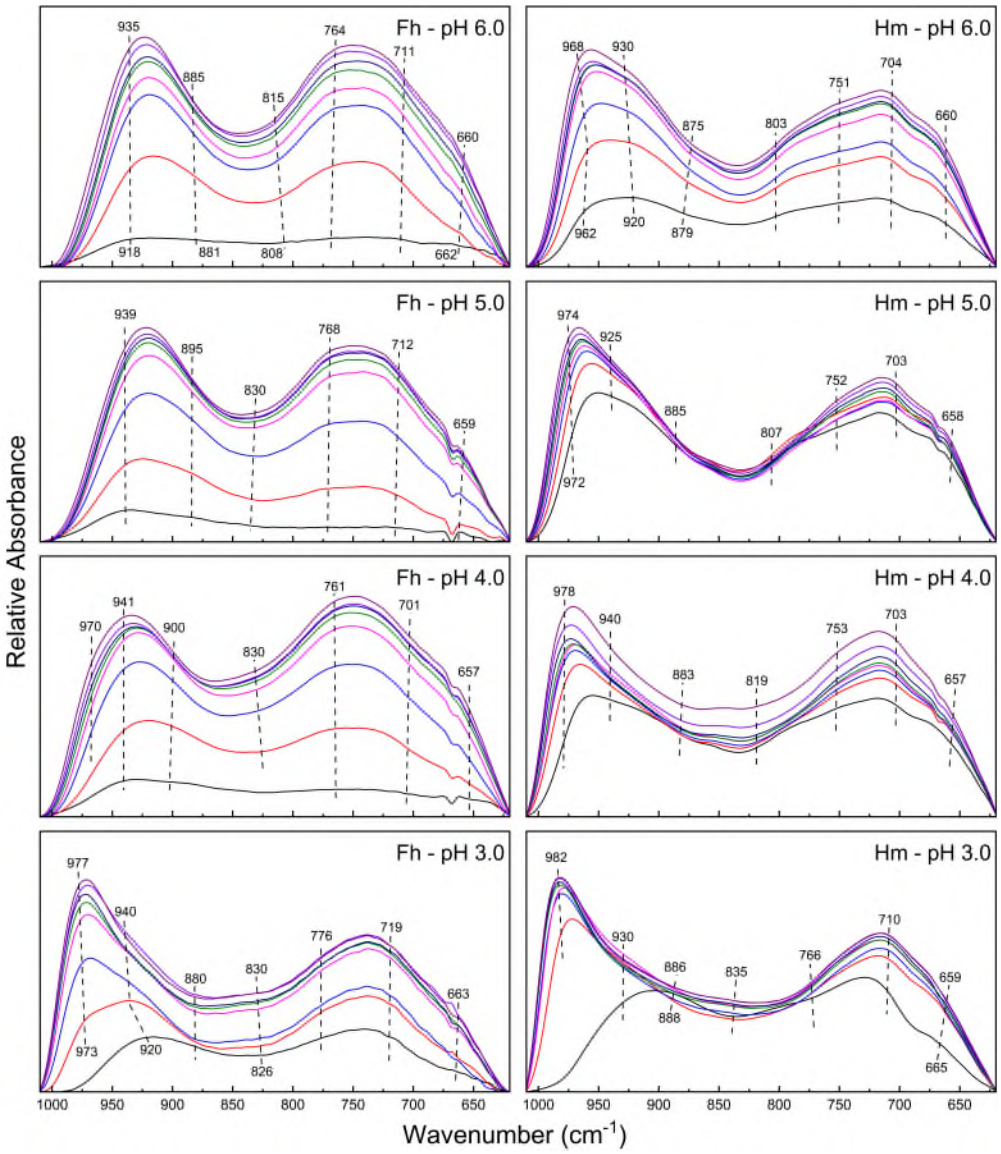

Figure 2. ATR-FTIR spectra of sorbed V(V) onto ferrihydrite (left column) and hematite (right column) from 50 (bottom) to 5000 (top) µM for each pH value. Dashed lines with wavenumbers denote peak positions identified using the 2nd derivative and deconvolution peak fitting for spectra collected at 5000 µM.

In contrast to ferrihydrite, adsorption onto hematite surfaces exhibits similar bands independent of pH and surface loadings. Spectra obtained at all experimental pH values exhibit bands at approximately 660, 704, 751, 803, 875, 930 and 968 cm^{-1}, which are present from low (50 µM) to high (5000 µM) $[V]_T$ (Figure 2). With increased surface loading and decreasing pH, the intensity of peaks at 930 and 968 cm^{-1} increased while bands between 620 to 800 cm^{-1} remain

relatively constant. However, at pH 3 bands at positions 660, 710, and 766 cm^{-1} dampen compared to similar bands at higher pH.

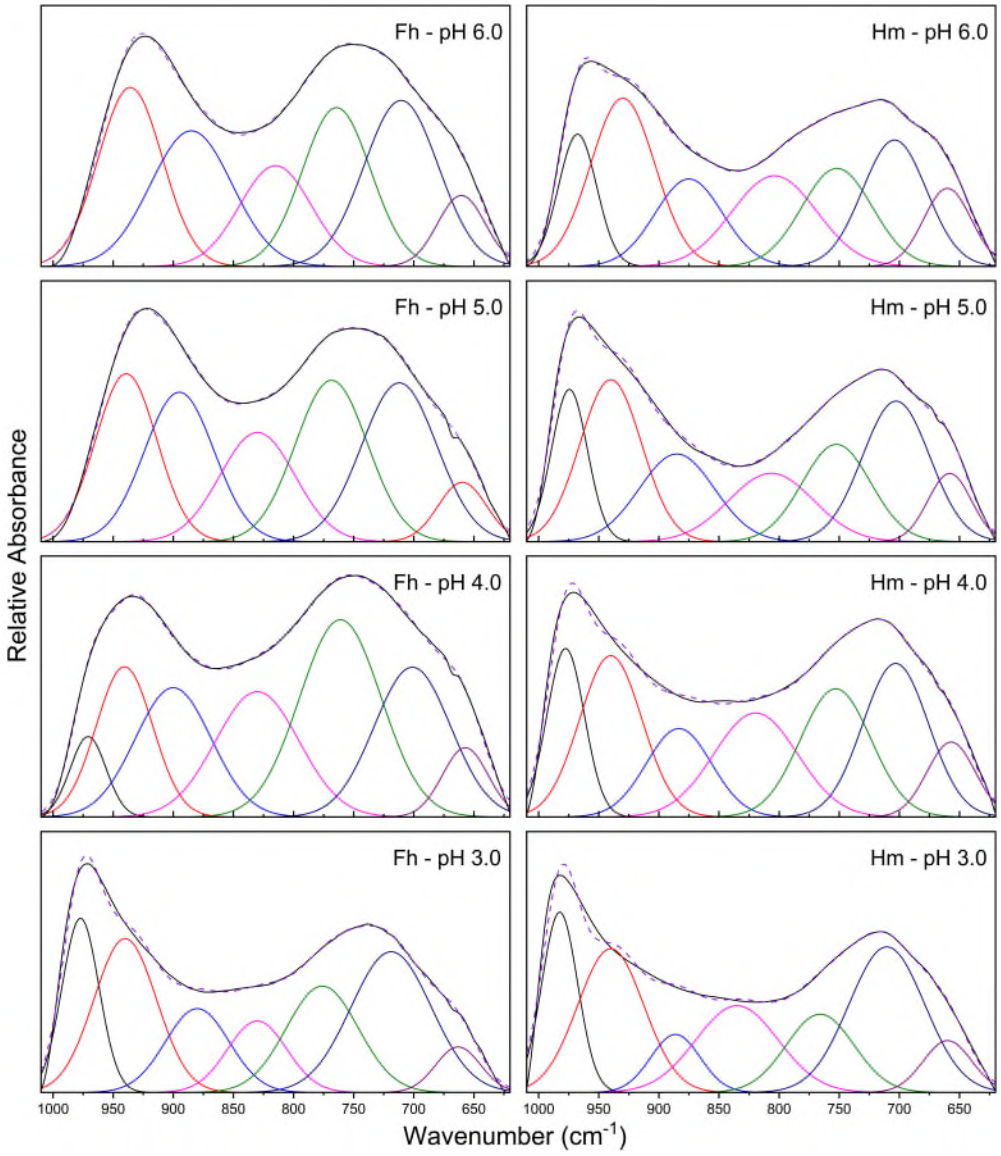

Figure 3. Decomposition of ATR-FIR spectra for adsorbed V(V) onto ferrihydrite (left column) and hematite (right column) at 5000 μM.

Adsorption Isotherms. Langmuir isotherm fits consistently show larger partitioning coefficients (K) for hematite than that for ferrihydrite (Table S3). Optimal isotherm fits for hematite

produced fit constants ranging from 0.012 to 0.100, whereas K values for ferrihydrite isotherms varied slightly between 0.005 and 0.007 (Table S3). These K values suggest that (poly)vanadates have a higher affinity for hematite surfaces compared to ferrihydrite. Isotherms for ferrihydrite experiments showed no apparent pH-dependent trends and produced coefficients consistent among all experiments (Figure 4a). Hematite adsorption isotherms displayed a decrease in K values from 0.100 to 0.023 corresponded to a pH decrease from 5 to 3. The pH 6 experiment for hematite does not follow this trend, however, the K value is similar to (poly)vanadate partitioning coefficients onto ferrihydrite at all experimental pH values. This result indicates that at pH 6, (poly)vanadate ions exhibit similar affinity for sorption onto hematite and ferrihydrite. At $[V]_T$ above 1000 μM and pH 4 and 5, normalized absorbance exhibits greater variability and isotherms are poorly described by the Langmuir model following reaction with hematite films (Figure 4b). This deviation from the fit at pH 4 and 5 may result from adsorption of multiple energetically heterogeneous species, which the Langmuir model cannot effectively describe.

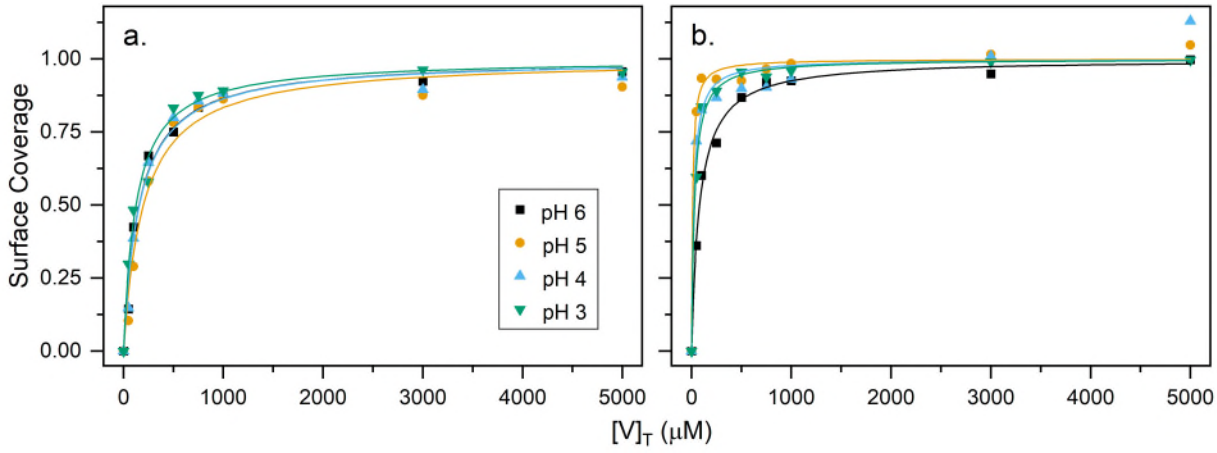

Figure 4. Integrated absorbance isotherms for ferrihydrite (a) and hematite (b) with modeled Langmuir isotherm fits (solid lines).

DISCUSSION

Aqueous (Poly)Vanadate Speciation. Previous studies have reported active Raman and IR bands for aqueous and adsorbed (poly)vanadate species on layered double hydroxide phases (Table 1). Features obtained from aqueous (poly)vanadate species observed in ATR-FTIR spectra from this study (Figure 1) can be interpreted by comparing relative proportions of each V(V) species with published values (Figure 5). This comparison indicates that VO_2^+, $[H_xV_{10}O_{28}]^{(6-x)-}$, chain-like forming species (i.e., $[H_xV_2O_7]^{(4-x)-}$ and $V_4O_{12}^{4-}$), and HVO_4^- dominate at pH 1, 4, 7, and 11, respectively. Under highly acidic conditions (i.e., pH < 2), VO_2^+ dominates and produces bands at 938, 1015, and 1187 cm^{-1} (Figure 1). Griffith and Lesniak (1969) ascribed bands at 920, and 940 cm^{-1} to VO_2^+ at pH 0.9, which is generally consistent with the weak band we observed at 938 cm^{-1} here. With a similar linear structure to the uranyl cation ($O=U=O^{2+}$), ATR-FTIR spectra for aqueous VO_2^+ spectra reflect asymmetric stretching of V=O bonds.[33,56]

Thermodynamic modeling predicts that $H_2VO_4^{2-}$ dominates between pH 5 and 9 when $[V]_T$ is below 1000 μM. However, at pH 6 the linear molecule $H_2V_2O_7^{2-}$ and cyclical $V_4O_{12}^{4-}$ polyvanadate species may constitute ~30 % of $[V]_T$ (Figure 5). This modeling also predicts that $H_2VO_4^-$, $H_2V_2O_7^{2-}$ and $V_4O_{12}^{4-}$ account for approximately 20, 15 and 60 % of aqueous V(V), respectively, where $[V]_T$ equals 5000 μM. Measured spectra (Figure 1) exhibit similar features to previously published IR spectra for both aqueous (Table 1). Bands at 834, 952, and 1066 cm^{-1} correspond to $H_2VO_4^-$, $H_2V_2O_7^{2-}$ and $V_4O_{12}^{4-}$, which are characterized by similar C_{2v} symmetry and V-O-V or V-O stretching modes.[55,57–60] As pH decreases the dominant species become $HV_{10}O_{28}^{6-}$, $H_3V_{10}O_{28}^{5-}$ and $NaHV_{10}O_{28}^{4-}$ (Figure 5) and can be attributed to bands at 842, 965 and 1016 cm^{-1}. Decavanadate and the $Mo_7O_{24}^{6-}$ polyoxyanion have similar structures with C_{2v}

symmetry in a distorted octahedral geometry and bands occurring between 800 and 1000 cm^{-1}.[20,37,38,55] Vanadate polymers decompose at pH above 10 to form the HVO_4^- oxyanion, which exhibits C_{3v} symmetry. The measured value of 861 cm^{-1} at pH 11 is consistent with HVO_4^- Raman and IR bands at 877 cm^{-1} (Table 1). Free T_d VO_4^{3-} only occurs at pH above 12, but similar to other aqueous oxyanion forming metals (e.g., Mo and W) this ion only produces a single band at ~830 cm^{-1} (Table 1).[35]

Table 1. Summary of dissolved V species band positions measured by Raman (*) and IR (†) spectroscopy. Peak positions for $H_2V_2O_7^{2-}$ and $V_4O_{12}^{4-}$ are reported with identical values as these species occur simultaneously in solution and cannot be determined separately. Metavanadate species included are $V_3O_{10}^{5-}$, $V_4O_{12}^{4-}$, $V_5O_{15}^{5-}$, and $V_6O_{18}^{6-}$.

References	VO_2^+	VO_4^{3-}	HVO_4^{2-}	$H_2VO_4^{2-}$	$[H_xV_2O_7]^{(4-x)-}$	Metavanadate	$H_xV_{10}O_{28}^{(6-x)-}$
a†	938, 1015, 1187		861	952	834, 952	834, 952, 1066	842, 965, 1016
b*		820	875		875	947	593, 967, 995
c†		336, 804, 826			360-464, 560, 760-790, 830-895, 915-950	646, 940	
d, e*		827	351, 545, 877	945	351, 503, 810, 850, 877	360, 884, 945	320, 454, 534, 595, 800, 834, 870, 960-998
f, g, h*†	920, 940	340, 780, 827	351, 545, 800, 877		210, 351, 503, 810, 850, 877, 915	330, 360, 490, 630, 905, 945	910, 955, 960, 990

a This study
b Aureliano et al. (2016)
c Salak et al. (2012)
d Twu and Dutta (1990)
e Twu and Dutta (1989)
f Griffith and Lesniak (1969)
g Griffith (1967)
h Griffith and Wickins (1966)

Attenuation of (Poly)Vanadate Species. Surface complexation of aqueous oxyanions alters the symmetry of the free species resulting in a lower symmetry.[35,43,44,63–65] Adsorption of V(V) with ferrihydrite produces four strong bands between 650 and 850 cm^{-1} that are pH-independent, and three distinct bands between 850 and 980 cm^{-1} that exhibit increasing relative intensity with

decreasing pH (Figures 2 and 3). Deconvolution and 2nd derivative analysis of ferrihydrite spectra reveal limited differences for pH 4, 5, and 6, whereas spectra collected at pH 3 exhibit a sharp increase in intensity at 970 cm^{-1} (Figure 3). At $[V]_T$ less than 500 µM, peaks are distinguishable at approximately 880 and 940 cm^{-1} suggesting the presence of minor amounts (~10 to 15%) of aqueous polynuclear V(V) species (Figure 2). Bands reflecting adsorption of polynuclear V species (i.e., 900, 940, and 970 cm^{-1}) increase in intensity at $[V]_T$ above 250 µM and with decreasing pH (Figure 3).[55,59,60] A concomitant decrease in band intensity at 650 and 850 cm^{-1} associated with tetrahedrally coordinated (poly)vanadate sorption is also apparent.

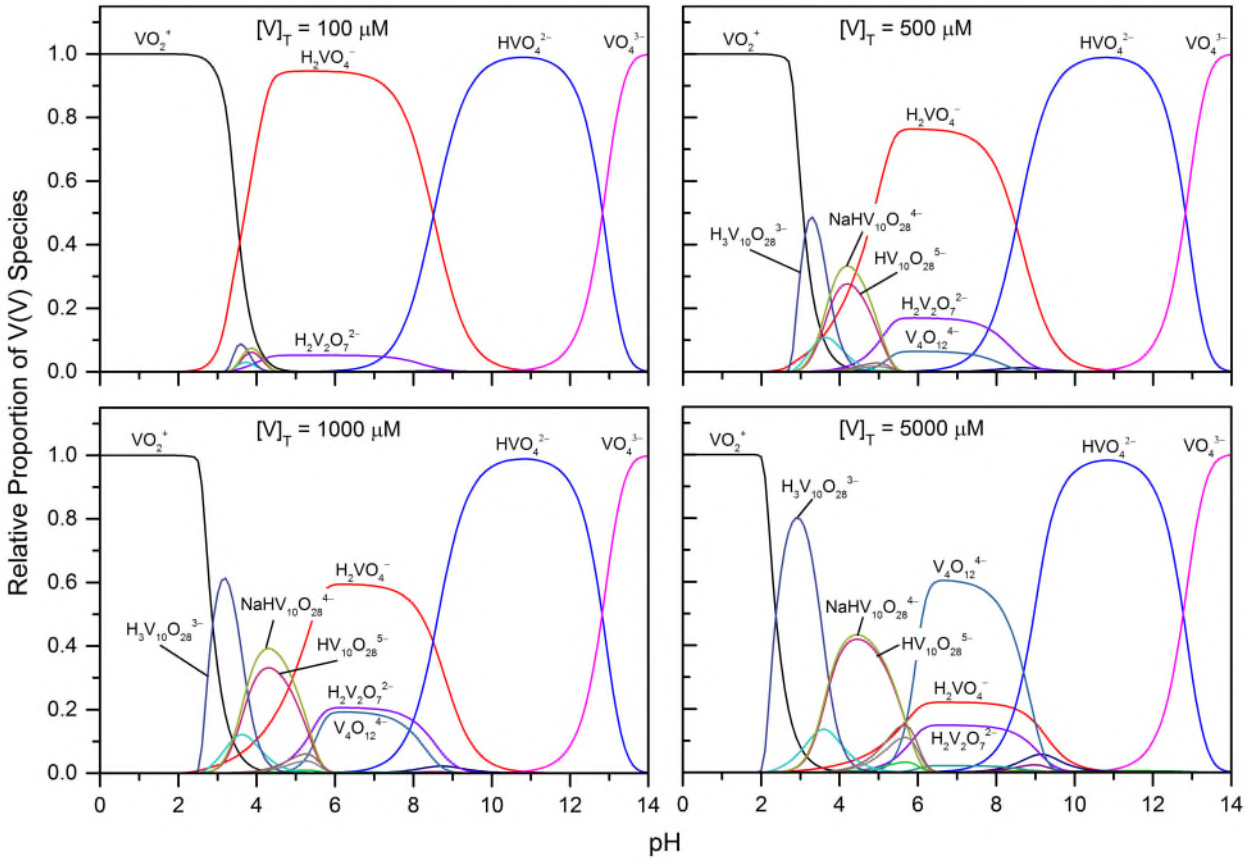

Figure 1. Aqueous V speciation diagrams at 100 (top left), 500 (top right), 1000 (bottom left), and 5000 (bottom right) µM based on compiled thermodynamic data.

Comparatively, surface adsorption of V at hematite surfaces produces sharper features with four main bands between 650 and 860 cm^{-1} and three bands between 850 and 950 cm^{-1} (Figure 2 and

3). Similar to adsorbed V spectra on ferrihydrite, bands at lower wavenumbers (650 to 860 cm^{-1}) result from surface complexation of tetrahedrally coordinated (poly)vanadate species. These features are generally sharper at pH 5 and 6 but weaken or disappear as pH decreases below 4 (Figure 2 and 3). The two dominant bands at approximately 930 and 970 cm^{-1} systematically increase in intensity with higher surface loadings. However, as pH decreases from 6 to 3 the peak at ~930 cm^{-1} is gradually dampened by the intense peak at 970 cm^{-1}.

When considering V(V) sorption onto ferrihydrite and hematite surfaces, the appearance and dampening of bands directly relates to aqueous (poly)vanadate speciation and surface complexation. The doubly protonated $H_2VO_4^-$ is the predominant aqueous species at $[V]_T$ less than 1000 μM and pH 5 to 6 (Figure 5). Assigning bands associated to V-O-Fe adsorption complexes on ferrihydrite and hematite surfaces is difficult due to the presence of several adsorption complexes, mixtures of adsorbed species, and the C_{2v} symmetry of $H_2VO_4^-$.[65] Adsorption of $H_2VO_4^-$ onto Fe(III) and Al(III) (oxyhydr)oxides results from formation of inner-sphere bidentate binuclear and mononuclear complexes.[22,23,25,26,29,66] Peaks associated with $H_2VO_4^-$ adsorption at pH 5 and 6 likely produce band splitting similar to bidentate surface complexation of arsenate ($H_2AsO_4^{2-}$) on (oxyhydr)oxides.[41,43,67] However, at increased concentrations, $H_2V_2O_7^{2-}$ and $V_4O_{12}^{4-}$ species dominate aqueous speciation (Figure 5). Adsorption of these polyvanadate species at hematite surfaces produces bands at 930 and 968 cm^{-1} that increase with $[V]_T$ (Figure 2 and 3). Indiscernible bands at 970 cm^{-1} at pH 5 and 6 suggests that ferrihydrite may have a limited ability for surface complexation of polyvanadate species, due to its more amorphous characteristics.[38] The high affinity of tetrahedrally coordinated V(V) species for Fe(III) (oxyhydr)oxide surfaces at circumneutral pH suggests that hematite is a suitable substrate for $H_2V_2O_7^{2-}$ and $V_4O_{12}^{4-}$ adsorption.[22,23,25,29] Adsorbed dimer

and tetramer polymers likely result from multiple monodentate bonds, since bidentate complexation would be sterically hindered.

From pH 5 to 3 and $[V]_T$ above 250 μM, $HV_{10}O_{28}^{6-}$, $NaHV_{10}O_{28}^{5-}$ and $H_3V_{10}O_{28}^{5-}$ polynuclear species are thermodynamically predicted to be the dominant aqueous V(V) species (Figure 5). Increasing abundance of these species correspond to increasing IR band intensities between 970 and 980 cm^{-1}. However, ferrihydrite may be less thermodynamically favourable for adsorption of V(V) polynuclear species compared to the hematite (0001) crystal face due to the rigid and large decavanadate atomic structure. This hypothesis is supported by a higher number of bands attributed to complexation of polymeric species with hematite surfaces (Figure 3) and to higher affinity of (poly)vanadates for hematite based on Langmuir isotherms (Figure 4; Table S3). Preferential polymer formation at the hexagonal (0001) hematite crystal face compared to less crystalline Fe(III) (oxyhydr)oxides has previously been demonstrated for polynuclear Mo and W sorption.[34,38,68] Unlike polymolybdate, epitaxial growth of decavanadate on hematite is likely inhibited by its large structure.[38] However, previous studies have observed substitution of metavanadate and decavanadate species into layered-double hydroxides.[57–59] At concentrations below 250 μM, the oxycation VO_2^+ represents over 60% of $[V]_T$ at pH 3 (Figure 5). Uptake of VO_2^+ is likely limited due to the experimental pH being below the point of zero charge for Fe (oxyhydr)oxide surfaces, resulting in a net positive surface charge.[21] Adsorption of VO_2^+ at ferrihydrite and hematite surfaces likely includes outer-sphere interactions and potentially weak inner-sphere monodentate sorption. This observation is consistent with previous adsorption data for VO_2^+ onto goethite and δ-Al_2O_3 through ligand exchange of surficial hydroxyl groups.[26,66]

CONCLUSIONS

Previous studies have described vanadate adsorption onto ferrihydrite and goethite, yet uptake of polyvanadate species by Fe (oxyhydr)oxides have not yet been considered.[22,25,26,29] Investigation of (poly)vanadate interaction with ferrihydrite and hematite by ATR-FTIR revealed multiple bonding environments and inferred uptake mechanisms. Measured spectra coupled with thermodynamic modelling highlights the complex geochemical behaviour of aqueous V(V). At pH 5 and 6 at $[V]_T$ lower than 500 μm, $H_2VO_4^-$ adsorption produces multiple bands between 650 and 850 cm^{-1} indicating the formation of monodentate and bidentate surface complexes at both ferrihydrite and hematite surfaces. Bands at 930 and 970 cm^{-1} persist at elevated concentrations where tetrahedral coordinated $H_2V_2O_7^{2-}$ and $V_4O_{12}^{4-}$ form surface polymers at hematite. The lack of bands at 970 cm^{-1} in ferrihydrite spectra suggest surface polymer formation is limited. At pH 3 to 4, a strong band at ~980 cm^{-1} indicates the presence of adsorbed decavanadate on ferrihydrite and hematite. Adsorption of octahedrally coordinated decavanadate species at ferrihydrite and hematite surfaces are likely constrained to monodentate surface complexes due to is large and rigid structure. Similarly, adsorption of VO_2^+ at pH 3 and $[V]_T$ below 250 μM is limited to outer sphere and inner sphere monodentate adsorption.[26,66] Attenuation of polynuclear V(V) species is inhibited onto less crystalline Fe (oxyhydr)oxide surfaces (e.g., ferrihydrite, lepidocrocite, and goethite) at moderate pH conditions, which is consistent with previous studies for Mo and W polynuclear species.[34,38,68] The observed stability of aqueous V polynuclear species over a wide pH range (2 to 9) may have implications for V mobility within soils and sediments. Overall, these results demonstrate that (poly)vanadate species form surface polymers at ferrihydrite and hematite surfaces. Adsorption of V polymers at Fe(III) (oxyhydr)oxides have the potential to passivate reactive $Fe(O,OH)_6$ octahedra and could also inhibit uptake of nutrients

or metals.[38,39,41,69] Therefore, these reactions may have implications for V distribution and transport in terrestrial waters,[10] and use as a paleoredox indicator.[1]

ASSOCIATED CONTENT

Supporting Information

Compiled aqueous V reactions, and constants used for aqueous thermodynamic modelling are provided. In addition, two additional tables and two additional figures referenced in the text.

AUTHOR INFORMATION

ORCID

Colton J. Vessey: 0000-0003-3326-4216

Michael P. Schmidt: 0000-0001-8789-9204

Mojtaba Abdolahnezhad: 0000-0001-6695-8500

Derek Peak: 0000-0002-8876-3605

Matthew B. J. Lindsay: 0000-0001-9123-3261

Notes

The authors declare no competing financial interest.

Present Address

†Presently at Department of Earth and Atmospheric Sciences, University of Alberta, Edmonton, AB, T6G 2E3, Canada

ACKNOWLEDGEMENTS

Funding was provided by the Natural Sciences and Engineering Council of Canada (NSERC) through the Discovery Grants program (Grant No. RGPIN-2014-06589). Additional support

awarded to CJV through NSERC – Canada Graduate Scholarship – Masters (NSERC CGS-M) Program. MPS would like to acknowledge the Natural Sciences and Engineering Research Council Collaborative Research and Training Experience Sustainable Applied Fertilizer and Environmental Remediation (NSERC CREATE SAFER) program as well as an NSERC Research and Development grant supported by Federated Cooperatives Limited for financial support. We thank J.P. Gustafsson and D.L. Parkhurst for assistance with geochemical modelling and J.G. Hamilton for synthesizing the hematite used in this study.

REFERENCES

(1) Tribovillard, N.; Algeo, T. J.; Lyons, T.; Riboulleau, A. Trace Metals as Paleoredox and Paleoproductivity Proxies: An Update. *Chem. Geol.* **2006**, *232*, 12–32.
(2) Shaheen, S. M.; Alessi, D. S.; Tack, F. M. G.; Ok, Y. S.; Kim, K. H.; Gustafsson, J. P.; Sparks, D. L.; Rinklebe, J. Redox Chemistry of Vanadium in Soils and Sediments: Interactions with Colloidal Materials, Mobilization, Speciation, and Relevant Environmental Implications - A Review. *Adv. Colloid Interface Sci.* **2019**, *265*, 1–13.
(3) Babechuk, M. G.; Weimar, N. E.; Kleinhanns, I. C.; Eroglu, S.; Swanner, E. D.; Kenny, G. G.; Kamber, B. S.; Schoenberg, R. Pervasively Anoxic Surface Conditions at the Onset of the Great Oxidation Event: New Multi-Proxy Constraints from the Cooper Lake Paleosol. *Precambrian Res.* **2019**, *323* (December 2018), 126–163.
(4) Huang, J. H.; Huang, F.; Evans, L.; Glasauer, S. Vanadium: Global (Bio)Geochemistry. *Chem. Geol.* **2015**, *417*, 68–89.
(5) Wanty, R. B.; Goldhaber, M. B. Thermodynamics and Kinetics of Reactions Involving Vanadium in Natural Systems : Accumulation of Vanadium in Sedimentary-Rocks. *Geochim. Cosmochim. Acta* **1992**, *56* (4), 1471–1483.
(6) Gustafsson, J. P. Vanadium Geochemistry in the Biogeosphere –Speciation, Solid-Solution Interactions, and Ecotoxicity. *Appl. Geochemistry* **2019**, *102* (January), 1–25.
(7) Watt, J. A. J.; Burke, I. T.; Edwards, R. A.; Malcolm, H. M.; Mayes, W. M.; Olszewska, J. P.; Pan, G.; Graham, M. C.; Heal, K. V.; Rose, N. L.; et al. Vanadium: A Re-Emerging Environmental Hazard. *Environ. Sci. Technol.* **2018**, *52* (21), 11973–11974.
(8) Larsson, M. A.; Baken, S.; Gustafsson, J. P.; Hadialhejazi, G.; Smolders, E. Vanadium Bioavailability and Toxicity to Soil Microorganisms and Plants. *Environ. Toxicol. Chem.* **2013**, *32* (10), 2266–2273.
(9) Schlesinger, W. H.; Klein, E. M.; Vengosh, A. Global Biogeochemical Cycle of Vanadium. *Proc. Natl. Acad. Sci.* **2017**, *114* (52), E11092–E11100.
(10) Aureliano, M.; Crans, D. C. Decavanadate (V10O286-) and Oxovanadates: Oxometalates with Many Biological Activities. *J. Inorg. Biochem.* **2009**, *103* (4), 536–546.
(11) Aureliano, M.; Fraqueza, G.; Ohlin, C. A. Ion Pumps as Biological Targets for Decavanadate. *Dalt. Trans.* **2013**, *42* (33), 11770–11777.
(12) USEPA. US Environmental Protection Agency Drinking Water Contaminant Candidate

List 4 (CCL4) https://www.epa.gov/ccl/chemical-contaminants-ccl-4.
(13) Environment and Climate Change Canada. Canadian Environmental Protection Act (1999). Federal Environmental Quality Guidelines: Vanadium http://www.ec.gc.ca/ese-ees/default.asp?lang=En&n=48D3A655-1.
(14) RIVM Letter Report 601714021/2012; National Institute for Public Health and the Environment, B. *Environmental Risk Limits for Vanadium in Water: A Proposal for Water Quality Standards in Accordance with the Water Framework Directive*; 2012.
(15) Nesbitt, J. A.; Lindsay, M. B. J. Vanadium Geochemistry of Oil Sands Fluid Petroleum Coke. *Environ. Sci. Technol.* **2017**, *51* (5), 3102–3109.
(16) Hudson-Edwards, K. A.; Byrne, P.; Bird, G.; Brewer, P. A.; Burke, I. T.; Jamieson, H. E.; MacKlin, M. G.; Williams, R. D. Origin and Fate of Vanadium in the Hazeltine Creek Catchment Following the 2014 Mount Polley Mine Tailings Spill in British Columbia, Canada. *Environ. Sci. Technol.* **2019**, *53* (8), 4088–4098.
(17) Burke, I. T.; Mayes, W. M.; Peacock, C. L.; Brown, A. P.; Jarvis, A. P.; Gruiz, K. Speciation of Arsenic, Chromium, and Vanadium in Red Mud Samples from the Ajka Spill Site, Hungary. *Environ. Sci. Technol.* **2012**, *46* (6), 3085–3092.
(18) Baes, C. F.; Mesmer, R. E. *The Hydrolysis of Cations*; John Wiley & Sons, 1976.
(19) Chen, G.; Liu, H. Understanding the Reduction Kinetics of Aqueous Vanadium(V) and Transformation Products Using Rotating Ring-Disk Electrodes. *Environ. Sci. Technol.* **2017**, *51* (20), 11643–11651.
(20) Cruywagen, J. J. Protonation, Oligomerization, and Condensation Reaction of Vanadate(V), Molybdate(VI), and Tungstate(VI). *Adv. Inorg. Chem.* **1999**, *49*, 127–182.
(21) Cornell, R. M.; Schwertmann, U. *The Iron Oxides: Structure, Properties, Reactions, Occurences and Uses*; Wiley-VCH: Weinheim, 2003.
(22) Brinza, L.; Vu, H. P.; Neamtu, M.; Benning, L. G. Experimental and Simulation Results of the Adsorption of Mo and V onto Ferrihydrite. *Sci. Rep.* **2019**, *9* (1), 1365.
(23) Brinza, L.; Vu, H. P.; Shaw, S.; Mosselmans, J. F. W.; Benning, L. G. Effect of Mo and V on the Hydrothermal Crystallization of Hematite from Ferrihydrite: An in Situ Energy Dispersive X-Ray Diffraction and X-Ray Absorption Spectroscopy Study. *Cryst. Growth Des.* **2015**, *15* (10), 4768–4780.
(24) Kaur, N.; Singh, B.; Kennedy, B. J.; Gräfe, M. The Preparation and Characterization of Vanadium-Substituted Goethite: The Importance of Temperature. *Geochim. Cosmochim. Acta* **2009**, *73* (3), 582–593.
(25) Larsson, M. A.; Persson, A. I.; Sjo, B. C.; Gustafsson, J. P. Vanadate Complexation to Ferrihydrite : X-Ray Absorption Spectroscopy and CD-MUSIC Modelling. *Environ. Chem.* **2017**, *14*, 141–150.
(26) Peacock, C. L.; Sherman, D. M. Vanadium(V) Adsorption onto Goethite (α-FeOOH) at PH 1.5 to 12: A Surface Complexation Model Based on Ab Initio Molecular Geometries and EXAFS Spectroscopy. *Geochim. Cosmochim. Acta* **2004**, *68* (8), 1723–1733.
(27) Schwertmann, U.; Pfab, G. Structural Vanadium in Synthetic Goethite. *Geochim. Cosmochim. Acta* **1994**, *58* (20), 4349–4352.
(28) White, A. F.; Peterson, M. L. Reduction of Aqueous Transition Metal Species on the Surfaces of Fe(II) -Containing Oxides. *Geochim. Cosmochim. Acta* **1996**, *60* (20), 3799–3814.
(29) Vessey, C. J.; Lindsay, M. B. J. Aqueous Vanadate Removal by Iron(II)-Bearing Phases under Anoxic Conditions. *Environ. Sci. Technol.* **2020**, *In Review,* es-2019-06250j.

(30) Brinza, L.; Benning, L. G.; Statham, P. J. Adsorption Studies of Mo and V onto Ferrihydrite. *Mineral. Mag.* **2008**, *72* (1), 385–388.
(31) Mayes, W. M.; Jarvis, A. P.; Burke, I. T.; Walton, M.; Feigl, V.; Klebercz, O.; Gruiz, K. Dispersal and Attenuation of Trace Contaminants Downstream of the Ajka Bauxite Residue (Red Mud) Depository Failure, Hungary. *Environ. Sci. Technol.* **2011**, *45* (12), 5147–5155.
(32) Wisawapipat, W.; Kretzschmar, R. Solid Phase Speciation and Solubility of Vanadium in Highly Weathered Soils. *Environ. Sci. Technol.* **2017**, *51* (15), 8254–8262.
(33) Lefèvre, G.; Noinville, S.; Fédoroff, M. Study of Uranyl Sorption onto Hematite by in Situ Attenuated Total Reflection-Infrared Spectroscopy. *J. Colloid Interface Sci.* **2006**, *296* (2), 608–613.
(34) Davantès, A.; Costa, D.; Lefèvre, G. Molybdenum(VI) Adsorption onto Lepidocrocite (γ-FeOOH): In Situ Vibrational Spectroscopy and DFT+U Theoretical Study. *J. Phys. Chem. C* **2016**, *120* (22), 11871–11881.
(35) Davantès, A.; Lefèvre, G. In Situ Characterization of (Poly)Molybdate and (Poly)Tungstate Ions Sorbed onto Iron (Hydr)Oxides by ATR-FTIR Spectroscopy. *Eur. Phys. J. Spec. Top.* **2015**, *224* (9), 1977–1983.
(36) Davantès, A.; Costa, D.; Lefèvre, G. Infrared Study of (Poly)Tungstate Ions in Solution and Sorbed into Layered Double Hydroxides: Vibrational Calculations and In Situ Analysis. *J. Phys. Chem. C* **2015**, *119* (22), 12356–12364.
(37) Davantès, A.; Lefèvre, G. In Situ Real Time Infrared Spectroscopy of Sorption of (Poly)Molybdate Ions into Layered Double Hydroxides. *J. Phys. Chem. A* **2013**, *117* (48), 12922–12929.
(38) Davantes, A.; Costa, D.; Sallman, B.; Rakshit, S.; Lefevre, G. Surface Polymerization of Mo(VI) and W(VI) Anions on Hematite Revealed by in Situ Infrared Spectroscopy and DFT+U Theoretical Study. *J. Phys. Chem. C* **2017**, *121* (1), 324–332.
(39) Christl, I.; Brechbühl, Y.; Graf, M.; Kretzschmar, R. Polymerization of Silicate on Hematite Surfaces and Its Influence on Arsenic Sorption. *Environ. Sci. Technol.* **2012**, *46* (24), 13235–13243.
(40) Sun, J.; Bostick, B. C. Effects of Tungstate Polymerization on Tungsten(VI) Adsorption on Ferrihydrite. *Chem. Geol.* **2015**, *417*, 21–31.
(41) Hu, S.; Yan, W.; Duan, J. Polymerization of Silicate on TiO2 and Its Influence on Arsenate Adsorption: An ATR-FTIR Study. *Colloids Surfaces A Physicochem. Eng. Asp.* **2015**, *469*, 180–186.
(42) Mayordomo, N.; Foerstendorf, H.; Lützenkirchen, J.; Heim, K.; Weiss, S.; Alonso, U.; Missana, T.; Schmeide, K.; Jordan, N. Selenium(IV) Sorption onto γ-Al2O3 : A Consistent Description of the Surface Speciation by Spectroscopy and Thermodynamic Modeling. *Environ. Sci. Technol.* **2018**, *52* (2), 581–588.
(43) Myneni, S. C. B.; Traina, S. J.; Waychunas, G. A.; Logan, T. J. Experimental and Theoretical Vibrational Spectroscopic Evaluation of Arsenate Coordination in Aqueous Solutions, Solids, and at Mineral-Water Interfaces. *Geochim. Cosmochim. Acta* **1998**, *62* (19–20), 3285–3300.
(44) Peak, D.; Luther, G. W. I.; Sparks, D. ATR-FTIR Spectroscopic Studies of Boric Acid Adsorption on Hydrous Ferric Oxide. *Geochim. Cosmochim. Acta* **2003**, *67* (14), 2551–2560.
(45) Wang, X.; Wang, Z.; Peak, D.; Tang, Y.; Feng, X.; Zhu, M. Quantification of Coexisting

Inner- and Outer-Sphere Complexation of Sulfate on Hematite Surfaces. *ACS Earth Sp. Chem.* **2018**, *2* (4), 387–398.
(46) Al-Kady, A. S.; Gaber, M.; Hussein, M. M.; Ebeid, E. Z. M. Structural and Fluorescence Quenching Characterization of Hematite Nanoparticles. *Spectrochim. Acta - Part A Mol. Biomol. Spectrosc.* **2011**, *83* (1), 398–405.
(47) Gustafsson, J. P. Visual MINTEQ version.3.1 https://vminteq.lwr.kth.se/.
(48) Parkhurst, D. L.; Appelo, C. A. J. Description of Input and Examples for PHREEQC Version 3: A Computer Program for Speciation, Batch-Reaction, One-Dimensional Transport, and Inverse Geochemical Calculations. *In: Techniques and Methods 6-A43. U.S. Geological Survey, Denver, USA*. 2013, p 497.
(49) Cruywagen, J. J.; Heyns, J. B. B.; Westra, A. N. Protonation Equilibria of Mononuclear Vanadate: Thermodynamic Evidence for the Expansion of the Coordination Number in VO2+. *Inorg. Chem.* **1996**, *35* (6), 1556–1559.
(50) Elvingson, K.; González Baró, A.; Pettersson, L. Speciation in Vanadium Bioinorganic Systems. 2. An NMR, ESR, and Potentiometric Study of the Aqueous H+-Vanadate-Maltol System. *Inorg. Chem.* **1996**, *35* (11), 3388–3393.
(51) Larson, J. W. Thermochemistry of Vanadium(5+) in Aqueous Solutions. *J. Chem. Eng. Data* **1995**, *40* (6), 1276–1280.
(52) McCann, N.; Imle, M.; Hasse, H. Carbonate Complexes of Vanadate. *Polyhedron* **2015**, *95*, 81–85.
(53) McCann, N.; Wagner, M.; Hasse, H. A Thermodynamic Model for Vanadate in Aqueous Solution – Equilibria and Reaction Enthalpies. *Dalt. Trans.* **2013**, *42*, 2622–2628.
(54) Smith, R. M.; Martell, A. E.; Motekaitis, R. J. NIST Critically Selected Stability Constants of Metal Complexes Database. *NIST, Gaithersburg, MD, USA NIST standard reference database 46, version 8.0*. 2004.
(55) Griffith, W. P.; Lesniak, P. J. B. Raman Studies on Species in Aqueous Solutions. Part III. Vanadates, Molybdates, and Tungstates. *J. Chem. Soc. A Inorganic, Phys. Theor.* **1969**, No. 0, 1066–1071.
(56) Gückel, K.; Tsushima, S.; Foerstendorf, H. Structural Characterization of the Aqueous Dimeric Uranium(vi) Species: (UO2)2CO3(OH)3-. *Dalt. Trans.* **2013**, *42* (28), 10172–10178.
(57) Twu, J.; Dutta, P. K. Decavanadate Ion-Pillared Hydrotalcite: Spectroscopic Studies of the Thermal Decomposition Process. *J. Catal.* **1990**, *124* (2), 503–510.
(58) Twu, J.; Dutta, P. K. Structure and Reactivity of Oxovanadate Anions in Layered Lithium Aluminate Materials. *J. Phys. Chem.* **1989**, *93* (23), 7863–7868.
(59) Salak, A. N.; Tedim, J.; Kuznetsova, A. I.; Ribeiro, J. L.; Vieira, L. G.; Zheludkevich, M. L.; Ferreira, M. G. S. Comparative X-Ray Diffraction and Infrared Spectroscopy Study of Zn-Al Layered Double Hydroxides: Vanadate vs Nitrate. *Chem. Phys.* **2012**, *397* (1), 102–108.
(60) Griffith, W. P.; Wickins, T. D. Raman Studies on Species in Aqueous Solutions. Part I. The Vanadates. *J. Chem. Soc. A Inorganic, Phys. Theor.* **1966**, 1087–1090.
(61) Aureliano, M.; Ohlin, C. A.; Vieira, M. O.; Marques, M. P. M.; Casey, W. H.; Batista De Carvalho, L. A. E. Characterization of Decavanadate and Decaniobate Solutions by Raman Spectroscopy. *Dalt. Trans.* **2016**, *45* (17), 7391–7399.
(62) Griffith, W. P. Vibrational Spectra of Metaphosphates, Meta-Arsenates, and Metavanadates. *J. Chem. Soc. A Inorganic, Phys. Theor.* **1967**, No. 0, 905–908.

(63) Hug, S. J. In Situ Fourier Transform Infrared Measurements of Sulfate Adsorption on Hematite in Aqueous Solutions. *J. Colloid Interface Sci.* **1997**, *188* (2), 415–422.
(64) Peak, D.; Ford, R. G.; Sparks, D. L. An in Situ ATR-FTIR Investigation of Sulfate Bonding Mechanisms on Goethite. *J. Colloid Interface Sci.* **1999**, *218*, 289–299.
(65) Nakamoto, K. *Infrared and Raman Spectra of Inorganic and Coordination Compounds, Part B*, 5th Editio.; Wiley-Interscience, New York., 1997.
(66) Wehrli, B.; Stumm, W. Vanadyl in Natural Waters: Adsorption and Hydrolysis Promote Oxygenation. *Geochim. Cosmochim. Acta* **1989**, *53*, 69–77.
(67) Roddick-Lanzilotta, A. J.; McQuillan, A. J.; Craw, D. Infrared Spectroscopic Characterisation of Arsenate (V) Ion Adsorption from Mine Waters, Macraes Mine, New Zealand. *Appl. Geochemistry* **2002**, *17* (4), 445–454.
(68) Davantès, A.; Lefèvre, G. Molecular Orientation of Molybdate Ions Adsorbed on Goethite Nanoparticles Revealed by Polarized in Situ ATR-IR Spectroscopy. *Surf. Sci.* **2016**, *653*, 88–91.
(69) Swedlund, P. J.; Miskelly, G. M.; McQuillan, A. J. Silicic Acid Adsorption and Oligomerization at the Ferrihydrite - Water Interface: Interpretation of ATR-IR Spectra Based on a Model Surface Structure. *Langmuir* **2010**, *26* (5), 3394–3401.